Ocean Engineering 342 (2025) 122882

Contents lists available at ScienceDirect

Ocean Engineering

journal homepage: www.elsevier.com/locate/oceaneng

Research paper

Experimental and numerical investigation on welded aluminium plates under quasi-static indentation loads

Shuai Zong [a,b], Yue Lu [a], Kun Liu [a,*], Zili Wang [a], Bai-Qiao Chen [b], C. Guedes Soares [b]

[a] School of Naval Architecture and Ocean Engineering, Jiangsu University of Science and Technology, Zhenjiang, 212003, Jiangsu, China
[b] Centre for Marine Technology and Ocean Engineering (CENTEC), Instituto Superior Técnico, Universidade de Lisboa, 1049-001, Lisbon, Portugal

ARTICLE INFO

Keywords:
Aluminium alloy
Butt weld
HAZ softening
Impact test
Numerical simulation

ABSTRACT

The impact responses of welded aluminium plates made from AA6061-T6 are systematically examined through experimental testing and numerical simulation, with a focus on the softening phenomena in the heat-affected zone (HAZ). Specimens with different numbers of welds and impact points are designed to clarify how HAZ softening affects damage features. Hardness and tensile tests are conducted to identify the material properties near the welds, supplying critical data for the numerical models. Finite element simulations of the impact tests are performed, explicitly considering the softening zones near the welds, to analyze damage behavior under various impact scenarios. Additionally, conventional simplified modelling methods for HAZ softening are evaluated and systematically compared to thoroughly assess the accuracy and applicability of different numerical modelling techniques for welded aluminium plates subjected to impact loading.

1. Introduction

Shell plates are the main structural components of ships and offshore structures. Both these plates and their associated primary and secondary supporting members are vulnerable to abnormal events such as slamming, ice impacts, collisions, and dropped objects on deck (Liu et al., 2015a, 2015b). Consequently, designing marine structures requires accurate prediction of the damage extent to plates subjected to lateral impacts, including evaluating permanent deformation and maximum indentation force, as well as assessing stress and strain distributions at both the impact site and the supports (Li et al., 2020; Liu et al., 2014).

Aluminium alloy is seen as a very promising choice for marine structures, especially for high-speed crafts, because of its low density, high energy absorption capacity, and excellent thermal conductivity (Mazzolani et al., 2014; Kaufman, 2000; Liu et al., 2022). However, the current design rules for aluminium ship structures mainly come from experiences with steel structures, and there is relatively limited data and practical experience for designing aluminium structures, particularly under accidental loading conditions (Villavicencio et al., 2012; Liu et al., 2015b; Li et al., 2020).

Aluminium alloys have lower Young's modulus and strength compared to steel, which leads to decreased stiffness and earlier plastic collapse (Gupta et al., 2020). Additionally, previous research has shown that aluminium alloys generally display anisotropic mechanical properties, with behavior depending on the loading direction relative to the material's principal axes, making impact modeling for aluminium structures more complex (Dunand et al., 2012; Rahmaan et al., 2020; Koubaa et al., 2016; Quach and Kim, 2021). Of particular importance is the softening effect in the heat-affected zone (HAZ) adjacent to welds, which requires special attention in shipbuilding. The welding process and subsequent cooling cause significant mechanical changes in the area surrounding the weld. Because the thermal expansion coefficient of aluminium alloys is roughly twice that of steel ($12 \times 10^{-6}\ ^{\circ}C^{-1}$), the HAZ in aluminium experiences more significant thermal variations (Hosseinabadi et al., 2021; Rønning et al., 2010; Magoga and Flockhart, 2014; Chen et al., 2024; Chen and Guedes Soares, 2019; Khedmati et al., 2014; Chan et al., 2014). As a result, aluminium near welds undergoes a greater reduction in strength as temperature increases compared to steel. It is understood that these weaker regions can considerably impact the load-carrying capacity of aluminium structures, highlighting the need for a detailed understanding of the local properties near welds, especially in the context of limit-state design approaches.

Modeling HAZ softening in finite element simulations depends on two main factors: the severity of strength reduction and the extent of the HAZ (Khedmati et al., 2014; Chan et al., 2014). The type of parent material mainly influences the level of strength loss in the HAZ. For

* Corresponding author.
E-mail address: kunliu@just.edu.cn (K. Liu).

https://doi.org/10.1016/j.oceaneng.2025.122882
Received 15 April 2025; Received in revised form 29 August 2025; Accepted 15 September 2025
Available online 24 September 2025

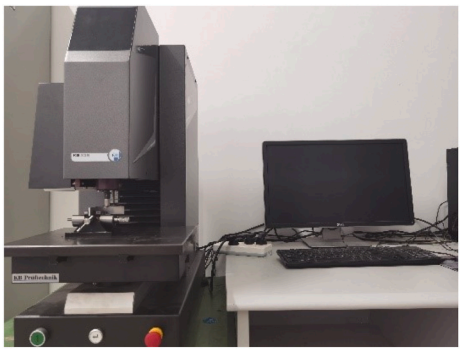

Fig. 1. Vickers micro-hardness tester.

standard aluminum alloys used in shipbuilding with fusion welding, this reduction is usually assumed to be 30–50 % of the base material's strength (Collette, 2005; ABS, 2012). In studies of the ultimate strength of stiffened aluminum panels, Zha and Moan (2001) and Paik and Duran (2004, 2005) used knock-down factors of 0.67 for 5083-H116 and 0.53 for 6082-T6, respectively. The American Bureau of Shipping (ABS, 2012) recommends a reduced proof strength of 0.77 for the HAZ in 5083-H116 aluminum alloy.

The extent of the HAZ, however, varies depending on different codes and standards. BS 8118 (British Standard, 1991) and Eurocode (British Standard, 2007) recommend a variable HAZ width based on joint geometry and welding process. DNV rules (Veritas, 2001) specify that the HAZ extends about three times the average thickness of the welded components on each side of the weld. A commonly used method to estimate the extent of softening is the "one-inch rule" (Lai, 1989), which states that the nominal HAZ extends 1 inch (25 mm) in all directions from a reference point in the weld. While this simplification is helpful for engineering uses, detailed measurements for various aluminum alloys, such as 6061-T6, are missing, and specific welding parameters are often not provided. Therefore, the trustworthiness of this rule when used on different types of welded aluminum structures remains uncertain, and more research is needed to understand the mechanical properties of aluminum alloys near the weld.

So far, few studies have systematically examined the softening effect of the heat-affected zone (HAZ) in aluminum structures exposed to accidental loads. Liu et al. (2020a, 2020b) experimentally and numerically studied the deformation and fracture behavior of welded 5083-H116 aluminum stiffened panels impacted by rigid hemispherical and semi-cylindrical indenters, emphasizing that ignoring joining details can greatly underestimate the reaction force and delay the start of structural failure. Cerik (2017) explored the response of fusion-welded AA5083-H116 rectangular plates with orthogonal stiffening under impulsive pressure, using simulations to assess how the HAZ negatively affects load capacity and ultimate failure under different impulses.

Morin et al. (2017) examined the impact response of stiffened aluminium panels with extruded profiles welded by friction stir welding, including HAZ softening by using a single set of material parameters with an assumed HAZ width of 20 mm. More recently, Li et al. showed that friction stir welding (FSW) of aluminium alloys produces a narrower, less severe HAZ and improves joint performance. (Li et al., 2024a; Li et al., 2024b; Li et al., 2024c). However, they did not provide

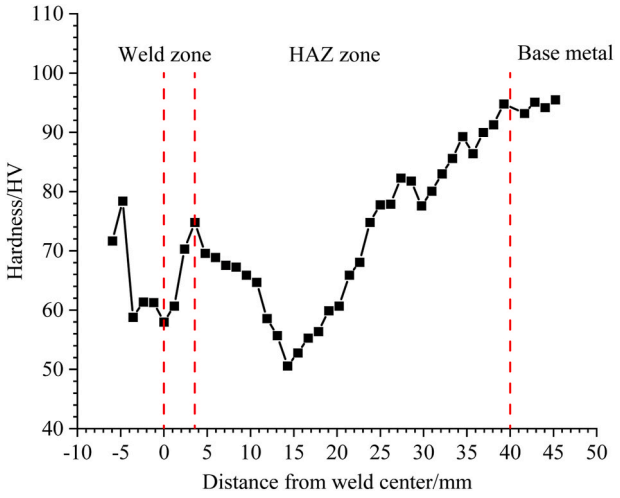

Fig. 3. Hardness profile for the welded specimens.

detailed descriptions of weld and HAZ characteristics, and this method is only valid if no fracture occurs within the HAZ. Despite these limitations, existing studies recognize that the under-matched HAZ in welded aluminium structures can accumulate plastic strain more quickly, which greatly affects limit state calculations. Therefore, with increasing demand for more accurate predictions, there is a need to continually improve and validate HAZ softening models in impact simulations of aluminium structures.

As of 2023, the second-generation Eurocode 9 (EN 1999) has been published(CEN.,2023). Compared with the 2007 edition, the new suite primarily expands scope and improves harmonisation by introducing additional structural typologies (bridges, space roofs, aluminium–concrete composite), new connection types (including friction-stir welding), a new buckling material class with corresponding curves, and several informative annexes. Particularly relevant to the present study, Annex Q provides a procedure to delineate the extent of the heat-affected zone (HAZ) from hardness measurements. Since the reliability framework and partial safety factors remain unchanged and our work does not perform design checks but relies on experimentally measured material properties, the conclusions of this study are unaffected by the code revision. Our hardness-based identification and sub-zoning of the HAZ are fully consistent with the intent of EN 1999-1-1:2023 Annex Q.

This study offers a combined experimental and numerical investigation of welded AA6061-T6 aluminum plates subjected to quasi-static punching by a rigid hemispherical indenter. To examine the impact of HAZ softening on the response of welded aluminum plates, butt-welded specimens with different numbers of welds and impact locations were designed. Material tests were performed to determine the mechanical properties of regions near the welds, providing data for the simulations. Finite element simulations of the impact tests included detailed modeling of the softening zones close to the welds. Finally, various modeling approaches for the HAZ softening zones were used to predict different impact scenarios and evaluate the effectiveness of the modeling techniques for welded aluminum plates.

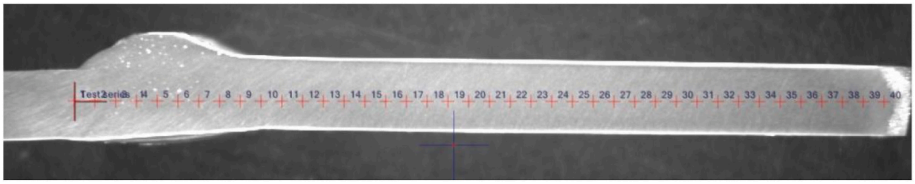

Fig. 2. Measuring points along butt weld.

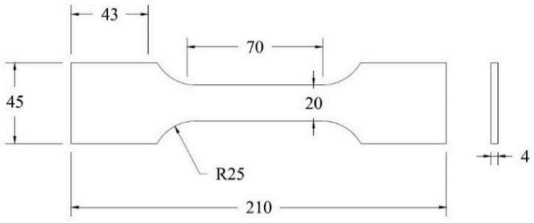

Fig. 4. Tensile test device and the dimensions of tensile coupons.

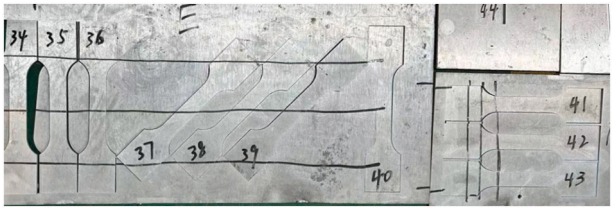

Fig. 5. Tensile specimens along different directions.

2. Material test

The impact specimens are made from AA6061 aluminum alloy in the T6 temper, one of the most common heat-treatable alloys used in shipbuilding. AA6061-T6 is a high-strength alloy available in various forms, including solid and hollow extrusions, tubes, plates, sheets, and forgings, and is increasingly used in structural components exposed to marine environments.

Specimens are produced using tungsten inert gas (TIG) butt welding, with ER4043 chosen as the filler material in accordance with Eurocode 9 ANNEX C (British Standard, 2007). The TIG welding is performed with a current of 165–175 A and a welding speed of 1 mm/s. High-purity argon gas acts as the shielding medium to avoid oxidation and contamination of the weld zone.

The mechanical properties of the welded specimens are assessed through hardness and tensile tests on samples taken from the same plate as the impact specimens, using identical welding parameters.

2.1. Hardness test

To quantitatively evaluate the material's strength, hardness tests were performed on the areas next to the butt weld according to GB/T 2654-2008, which outlines the standards for Vickers hardness testing of metal materials. The tests used a Vickers micro-hardness tester, as shown in Fig. 1, with a test load of 50 g and a dwell time of 10 s. Measurement points were arranged along the centerline of the weld cross-section, as shown in Fig. 2, with intervals of 1.19 mm based on the weld dimensions.

Note that the present hardness mapping and the identification of HAZ boundaries follow the philosophy later codified in EN 1999-1-1:2023 Annex Q, i.e., using the gradient and inflection points of the Vickers hardness profile across the weld to delineate the softening zone.

Fig. 3 shows the hardness profile of the welded specimen, with clear transitions in hardness values that help distinguish different zones. The area with a hardness around 100 HV corresponds to the base metal, matching the unwelded parent material and likely sharing similar mechanical properties. Next to the base metal is the heat-affected zone (HAZ), which is characterized by a significant decrease in hardness due to thermal exposure during welding. The innermost area is the weld zone, which is slightly thicker than both the HAZ and the base metal. The average hardness in the weld zone is slightly higher than in the HAZ.

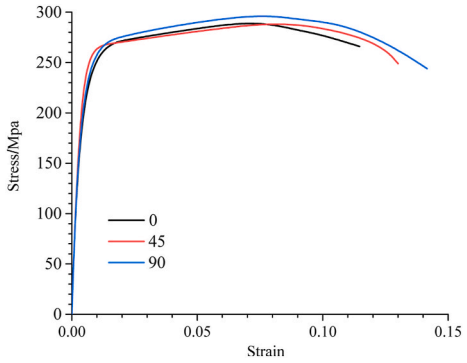

Fig. 6. Engineering stress-strain relationship along different directions.

Table 1
Characteristic mechanical properties for 6061 T6 aluminum alloys with thickness less than 12.5 mm in Eurocode 9.

Specification	Condition	Characteristic mechanical properties		
		0.2 % proof stress/MPa	Ultimate tensile stress/MPa	Minimum elongation/%
AA6061 T6	Base material	240	290	6
	HAZ	115	175	/

2.2. Tensile test on specimens with base material

Quasi-static tensile tests were conducted at a test speed of 1 mm/min to evaluate the mechanical properties of the aluminum alloy being studied. The test specimens were prepared according to GB/T 228.1–2010. Fig. 4 displays the tensile testing setup and the specimen dimensions.

To examine the anisotropic behavior of the aluminum alloy, tensile specimens were taken in three orientations—0°, 45°, and 90° relative to the rolling direction—as shown in Fig. 5. Each test was performed three times to verify the repeatability and reliability of the results.

Fig. 6 shows the engineering stress–strain curves for the three loading directions, with average values obtained from repeated tests. The mechanical properties of 6061-T6 aluminum alloy, as recommended by Eurocode 9, are also summarized in Table 1. The differences between the code-specified values and the experimental tensile results are minimal, demonstrating that the tensile test outcomes from this study are reliable.

The tensile results for the base material indicate that strain hardening behavior is similar in all three loading directions, while the failure strain shows slight variation. The highest ductility, with a value of 0.14, is observed in the direction perpendicular (90°) to the rolling direction. The degree of anisotropy in sheet materials is commonly quantified using the Lankford ratio r_α. This ratio is defined as the strain in the width direction divided by the strain in the through-thickness direction under uniaxial tension applied at an angle α relative to the rolling direction. The Lankford ratio can be expressed as:

$$r_\alpha = -\frac{\varepsilon_w^p}{\varepsilon_t^p} \tag{1}$$

where ε_w^p is the strain in the width direction and ε_t^p is the strain in the thickness direction, both of which can be determined from in-plane

Table 2
Lankford coefficient from different loading directions.

Loading direction/°	0	45	90
Lankford coefficient	0.58	0.55	0.60

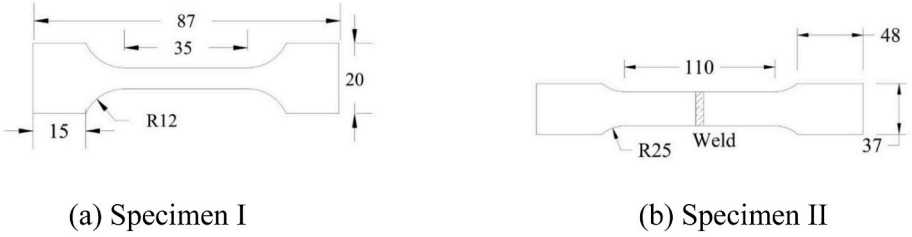

Fig. 7. Dimensions of the tensile specimens.

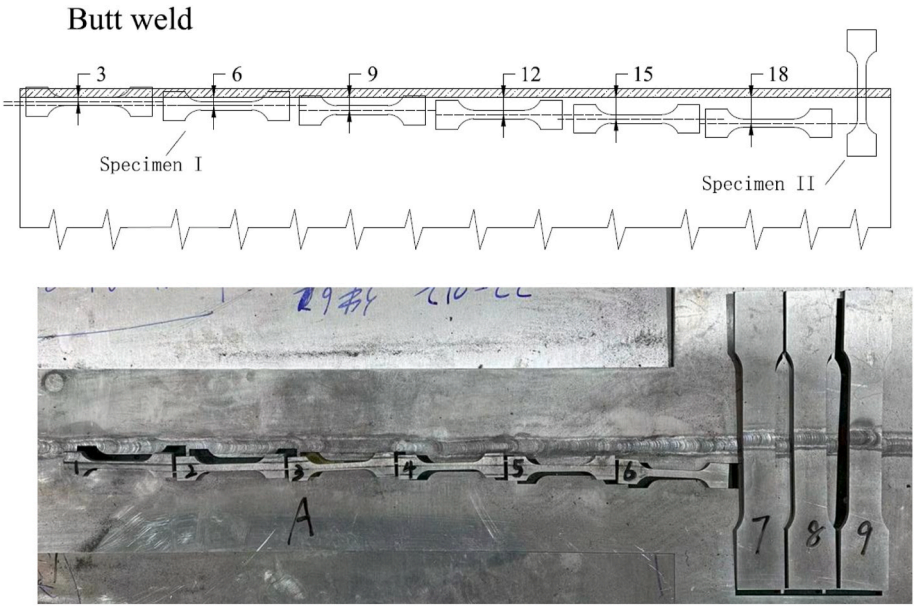

Fig. 8. Arrangement of specimens cut from the butt weld.

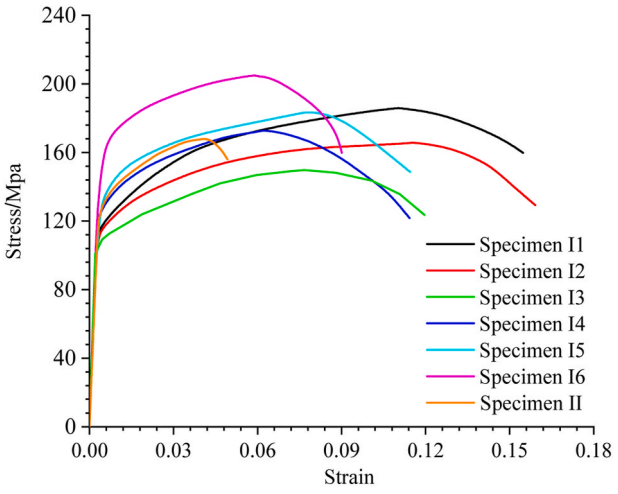

Fig. 9. Engineering stress-strain relationship for materials surrounding the weld.

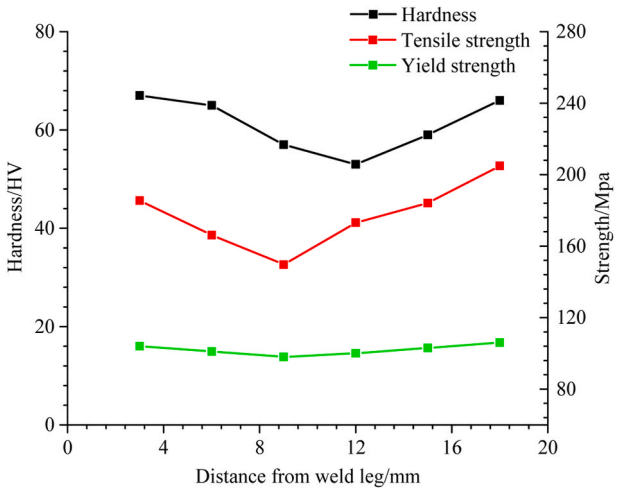

Fig. 10. Relationship between hardness and strength for HAZ materials.

strain measurements based on the plastic incompressibility condition. For a fully isotropic material, the Lankford parameter equals unity.

The Lankford coefficients were measured under different loading directions to assess the material's plastic anisotropy. The Lankford coefficient was determined to be 0.58 at 0°, 0.55 at 45°, and 0.60 at 90° relative to the rolling direction (see Table 2), indicating only moderate variation with respect to loading orientation. These results suggest that the investigated aluminium alloy exhibits minimal in-plane anisotropy, as the values are similar across directions. However, the coefficients being substantially lower than unity indicate significant anisotropy in the thickness direction.

2.3. Tensile test on specimens with welded part

A series of uniaxial tensile tests was conducted near the weld to evaluate the softening effect of the HAZ during the welding process,

(a) electro-hydraulic servo universal testing

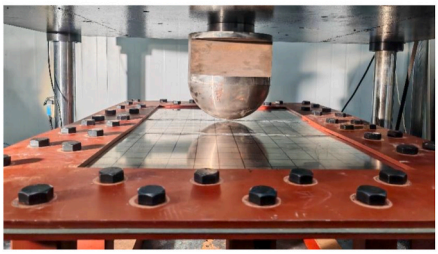

(b) Clamped specimen before testing

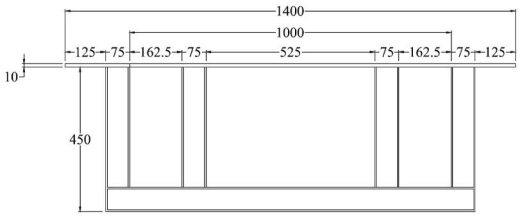

(c) Side view of the supporting base

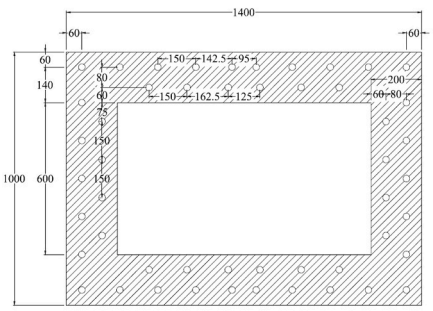

(d) Dimensions of the top frame

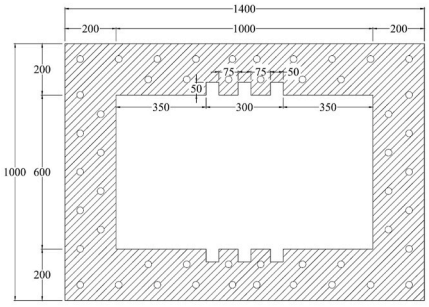

(e) Dimensions of the bottom frame

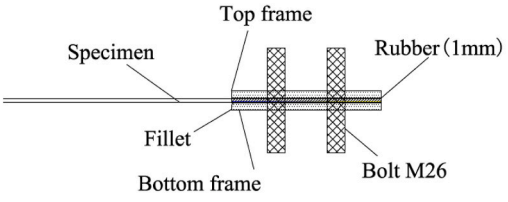

(f) Details of the cross-section of the boundary conditions

Fig. 11. Experimental set-up.

using the same welding parameters as those applied to the impact specimens. Two different sizes of tensile specimens were designed, as shown in Fig. 7, and are referred to as tensile specimen I (small size) and specimen II (large size) for clarity. Although the difference in size between Specimen I and Specimen II is not significant, their purposes are distinct. Specimen I was designed to systematically study the local mechanical property variations at different distances from the weld, while Specimen II aimed to represent the overall mechanical properties of the welded region under perpendicular loading. This distinction ensures that both local softening effects and global structural responses are adequately characterized.

The arrangement of the tensile specimens is illustrated in Fig. 8. For specimen I, the gauge width was set to 6 mm, with specimens cut parallel to the weld line at incremental distances of 3 mm from the weld. Six sets of tensile specimens were extracted from the plate around the butt weld, enabling the mechanical properties of the material within 18 mm of the weld to be characterized and the variation with respect to distance from the weld to be assessed.

Specimen II was designed with the weld seam oriented perpendicular to the loading direction, as also shown in Fig. 8. The weld joints were ground to smooth the surface to the same thickness as the plate (Liu et al., 2020a). Tensile tests performed on specimen II provide the

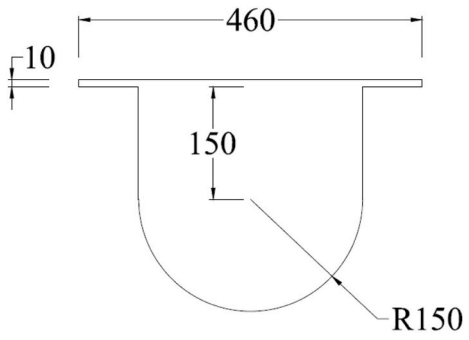

Fig. 12. Diagram of the impact indenter.

mechanical properties of the weakest zone in the welded specimen, which offers a straightforward, though approximate, method for assessing the softening zone's mechanical characteristics.

The engineering stress–strain curves obtained from the tensile specimens are shown in Fig. 9. A decrease in both yield and ultimate strength is seen in the HAZ material, along with a more noticeable strain hardening effect compared to the base material. This pattern is also apparent in the results from Specimen II, where the softening zone around the weld significantly reduces the overall strength and ductility of the welded specimen.

Additionally, the strength of the HAZ material does not increase linearly with distance from the weld seam; instead, it closely follows the hardness profile trend. Fig. 10 shows the relationship between hardness, strength, and distance from the weld for HAZ materials. Since the stress–strain curve for this material is more rounded than that of steel, the yield stress is defined using the 0.2 % offset proof stress. The results clearly indicate that the strength of the HAZ material decreases within about 9 mm of the weld center, then begins to increase as the distance grows. This effect is especially noticeable with tensile strength.

The present study mainly investigates the macro-mechanical response and softening phenomena at the engineering scale. Microscopic structural analysis, such as metallographic observation or scanning electron microscopy (SEM), would further clarify the relationship between microstructure and macroscopic mechanical properties. Because of equipment and scope limitations, such an analysis was not performed in this work, but it will be an important part of future research to connect the micro-macro mechanism.

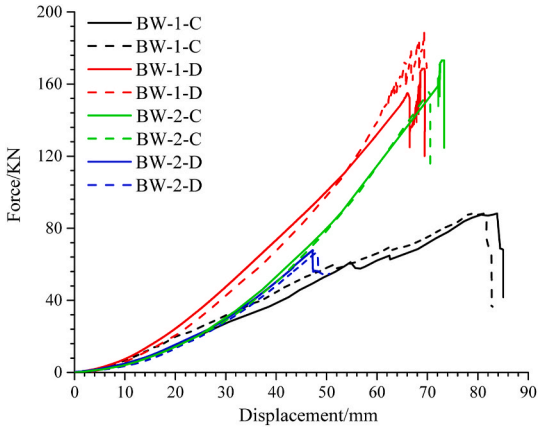

Fig. 14. Force-displacement responses from different indentation cases.

Table 3
Summary of the impact responses.

Indentation cases	Maximum force/KN	Fracture displacement/mm
BW-1-C	81	83
BW-1-D	166	67
BW-2-C	161	71
BW-2-D	67	47

3. Quasi-static impact test

3.1. Test set-up

Quasi-static tests were conducted using an electro-hydraulic servo universal testing machine (Fig. 11a). Deformation was applied via a hydraulic cylinder at a rate of 10 mm/min. A custom-designed supporting base (Fig. 11b and c) was used to ensure proper specimen support throughout the test. Force measurements were taken with a 100-ton load cell, while a 500 mm displacement transducer recorded the indenter's displacement. Panel deformation was visualized by applying a grid pattern with 10 × 10 mm squares to the specimen surface, and

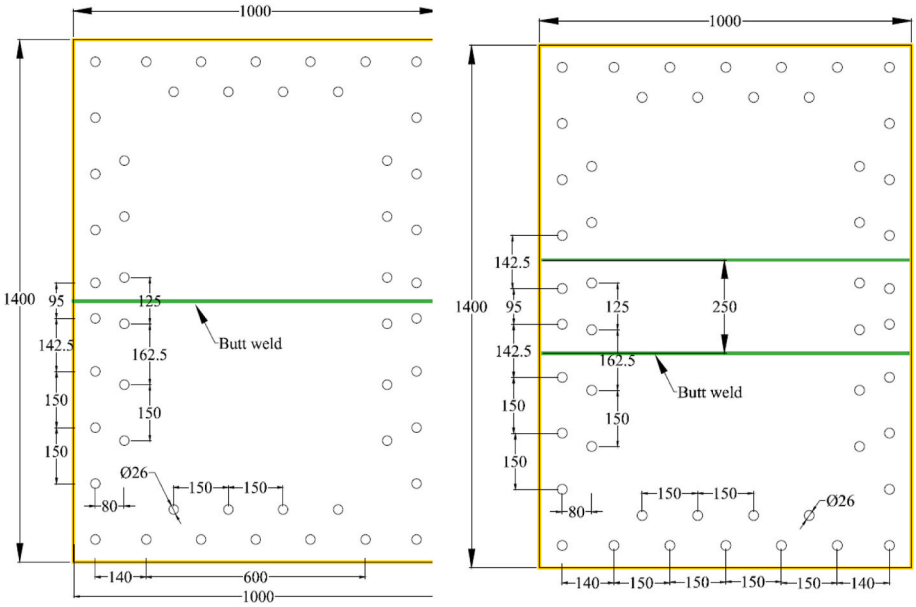

Fig. 13. Schematic diagram of the test specimens.

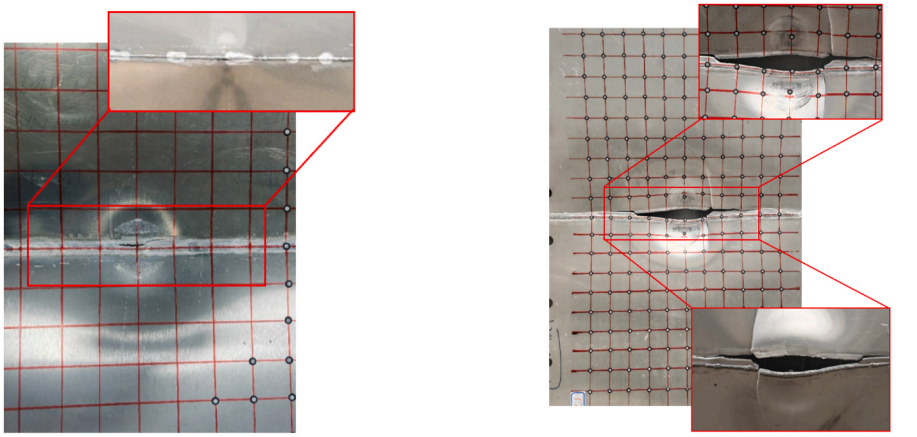

Fig. 15. Damage shapes in the BW-1-C case.

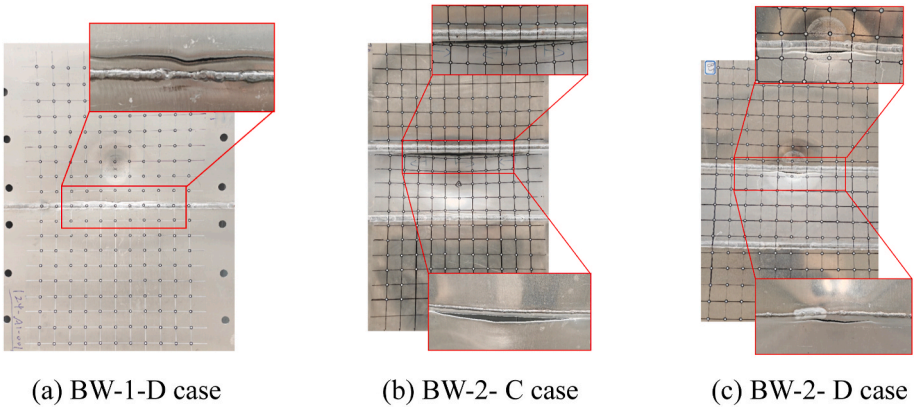

Fig. 16. Damage shapes in BW-1-D, BW-2- C, BW-2- D case.

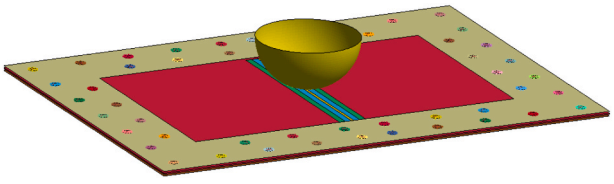

Fig. 17. Finite element model.

cameras positioned around the test rig monitored local deformation.

Before testing, specimens were mounted inside a test rig made of two large steel frames measuring 1400 mm × 1000 mm (Fig. 11d and e). The bottom frame was designed with a fillet next to the specimen to reduce strain concentration (Fig. 11f). To prevent sliding at the interfaces, a 1 mm thick rubber sheet was placed between the specimens and the frames. M26 bolts secured the plate tightly between the top and bottom frames during testing. The indenter (Fig. 12) consisted of a cylindrical body with a hemispherical end having a radius of 250 mm.

3.2. Specimen preparation and indentation cases

Fig. 13 shows the schematic diagram of the test specimens. Each specimen is a rectangular plate measuring 1400 mm × 1000 mm, made from 6061-T6 aluminum alloy with a thickness of 4 mm. The impact

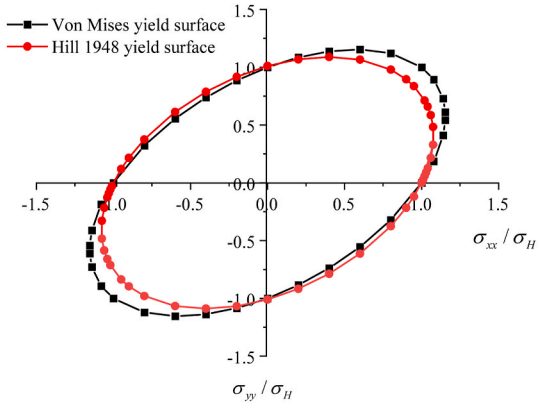

Fig. 18. Yield surfaces in plane stress plane.

Table 4
Anisotropic yield function parameters.

F	G	H
0.61	0.63	0.37
L	*M*	*N*
1.5	1.5	1.3

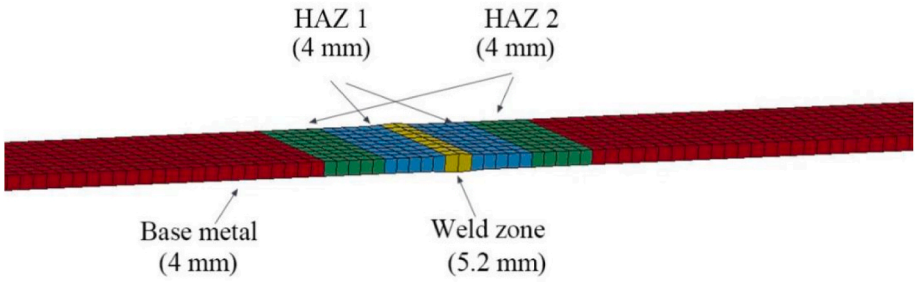

Fig. 19. Details of the modelling in the vicinity of the weld.

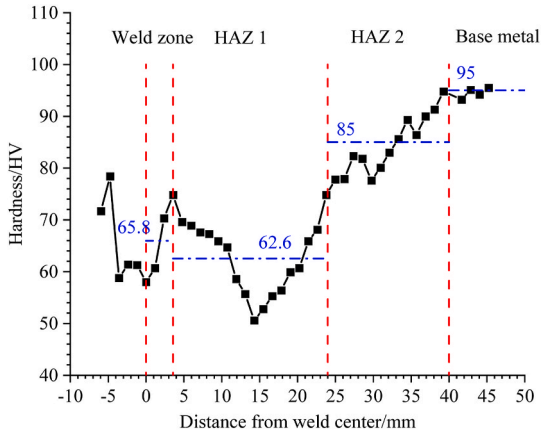

Fig. 20. The averaged hardness value for different zones around the weld.

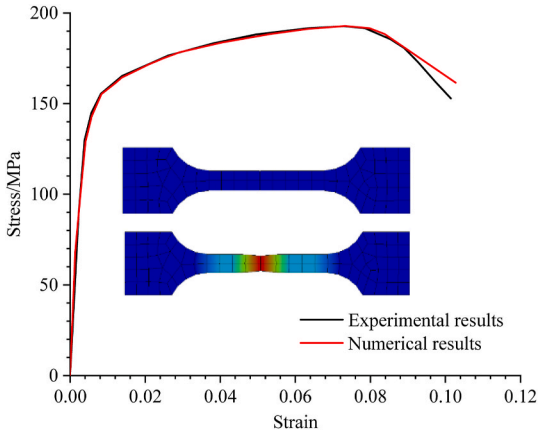

Fig. 22. Comparison of material curves from experimental and numerical results.

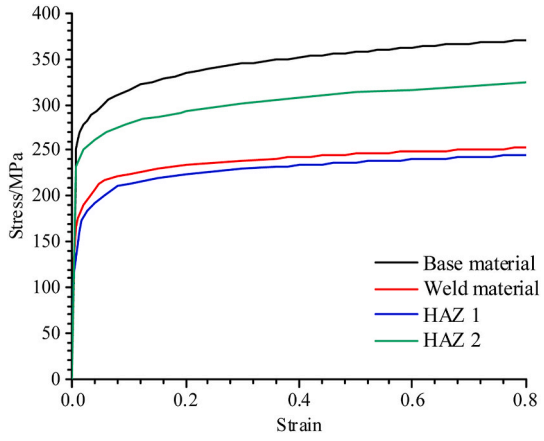

Fig. 21. The actual stress versus strain relationship for different zones around the weld.

area is 1000 mm × 600 mm, and grid lines were painted on the deformed side to help easily observe damage and deformation.

To study the effect of HAZ softening on impact response, specimens were prepared with different numbers of butt welds and impact locations. The specimens are made of precut plate parts joined with either one or two transverse butt welds using tungsten arc welding. Additionally, impact points were varied between the center of the specimen and a position offset by 125 mm from the center. For simplicity, each indentation case is labeled as BW-X-Y, where "BW" stands for butt weld, "X" indicates the number of welds (1 or 2), and "Y" shows the impact position—either center (C), 125 mm offset (D), HAZ-1 (H1), or HAZ-2 (H2).

3.3. Experimental results

The force–displacement responses from the quasi-static impact tests are shown in Fig. 14, with each indentation case involving two repeated tests. The results show minimal variation between repetitions in both stiffness and maximum force. Table 3 provides the average impact response values for all cases. It is clear that the presence of a weld seam significantly affects the impact responses of the specimens. Specimens display higher toughness under impact loading when the indenter does not directly contact the weld (BW-1-D and BW-2-C). In contrast, cases where the indenter impacts the weld, such as BW-2-D, show the lowest fracture displacement and structural resistance.

The deformation patterns for various indentation scenarios are shown in Figs. 15–18. When the welded specimen is impacted at the center of the weld seam (BW-1-C), significant ductile deformation occurs beneath the indenter. However, fracture initiates in the HAZ near the weld (Fig. 15a). At this stage, the beginning of cracking does not greatly affect the indentation force, as evidenced by only a slight drop at 51 mm displacement. Meanwhile, the specimen continues to support a substantial load. To better understand the damage process, testing was continued until a noticeable reduction in impact response was observed. As indentation progressed, the crack moved along the weld seam and then extended outward (Fig. 15b), causing a sharp drop in reaction force around 83 mm of indentation.

The damage morphology for the specimen with a single weld seam impacted at a 125 mm offset from the center (BW-1-D) is shown in Fig. 16. Significant stretching occurs beneath the indenter, and a necking circle, similar to that seen in unwelded specimens, is observed. Compared with BW-1-C, the structural stiffness is higher when the impact location is farther from the weld. However, fracture still begins in the HAZ next to the weld, with the crack propagating transversely as indentation increases.

For the specimen with two weld seams impacted at the center (BW-2-

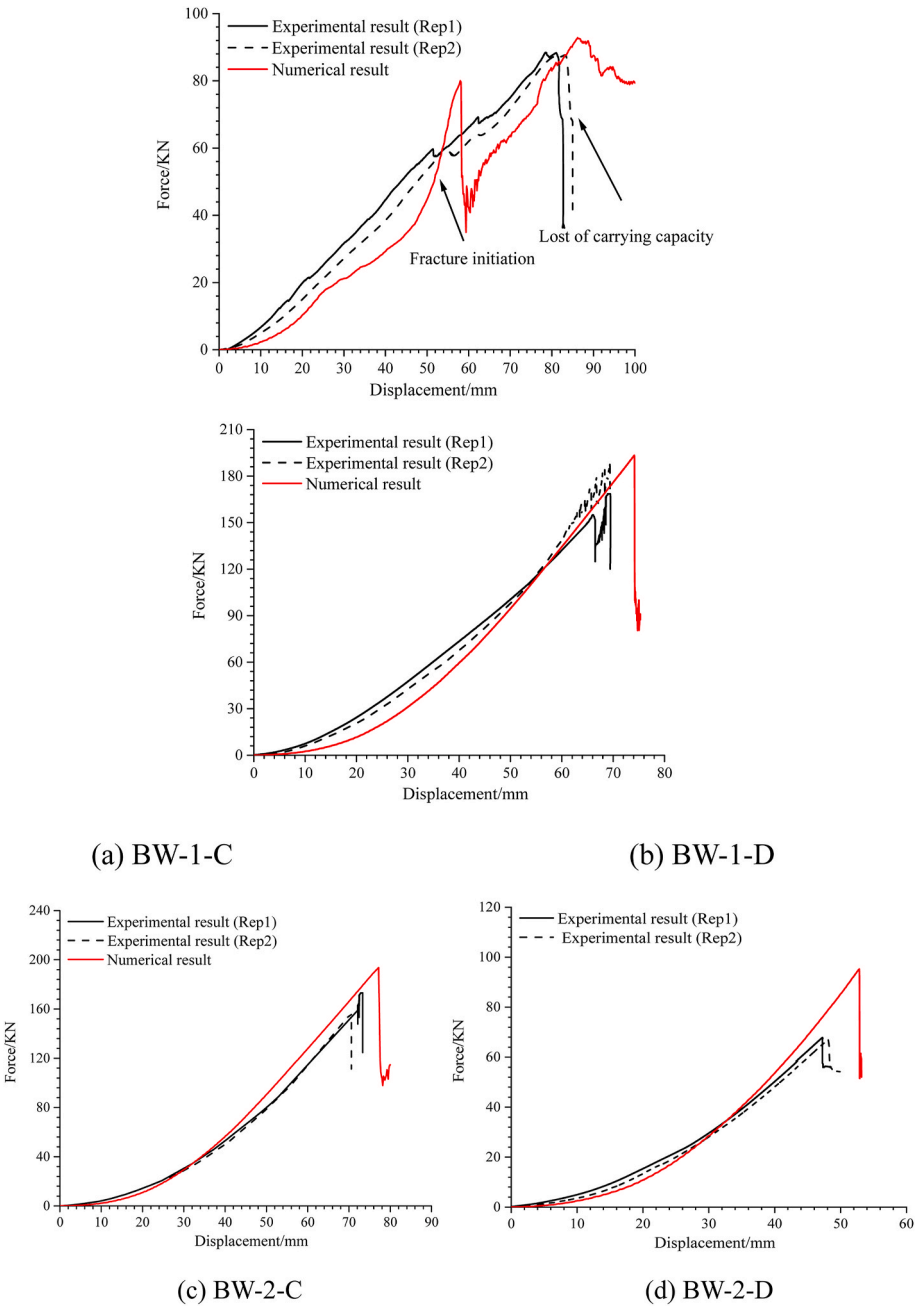

Fig. 23. Comparison of the impact responses.

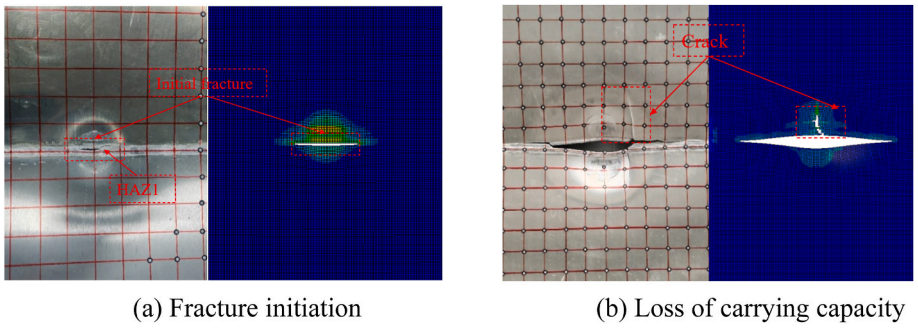

Fig. 24. Comparison of the damage shapes in BW-1-C.

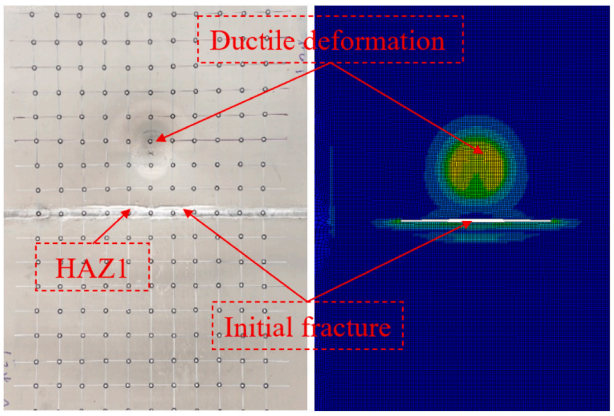

Fig. 25. Comparison of the damage shapes in BW-1-D.

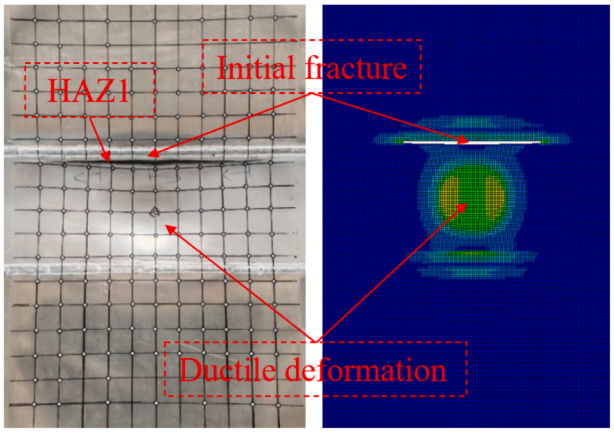

Fig. 26. Comparison of the damage shapes in BW-2-C.

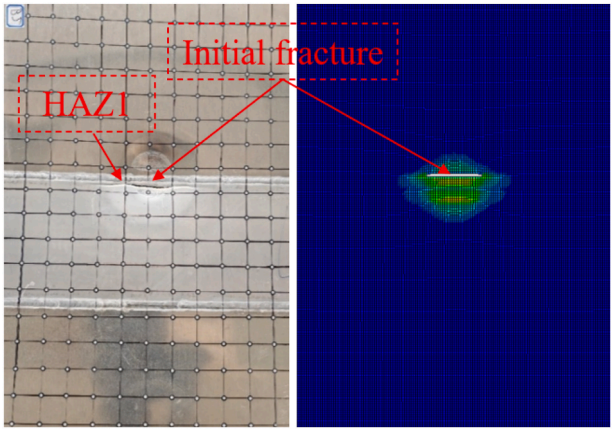

Fig. 27. Comparison of the damage shapes in BW-2-D.

C), plastic deformation remains confined to the area between the butt welds. Because the region between the two weld seams is weakened, the structural stiffness is lower compared to BW-1-D. Ultimately, the fracture begins in the HAZ on one side of the weld, with no fracture occurring in the weld metal itself.

When the specimen with two weld seams is indented directly at the weld seam (BW-2-D), a clear necking circle forms near the weld, and cracking occurs in the HAZ close to the inner side of the weld. This behavior is caused by the decreased structural strength in the area between the butt welds, making it more prone to fracture in that spot.

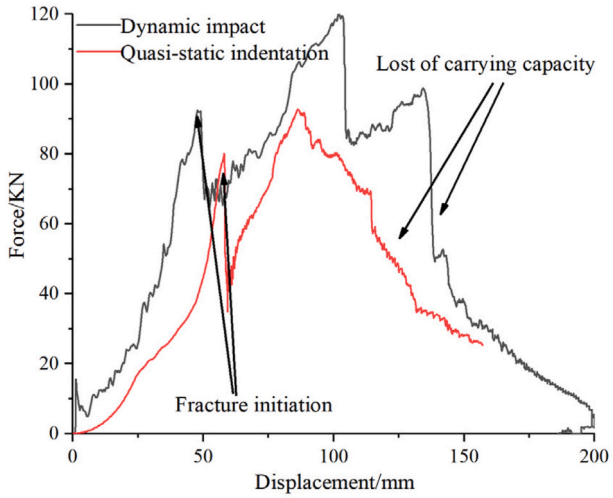

Fig. 28. The comparison of Force-Displacement Curves.

4. Numerical simulations

4.1. Finite element model

The computations were conducted using the explicit finite element code LS-DYNA. Fig. 17 shows the finite element model. Four-node shell elements with five through-thickness integration points were used, employing the Belytschko-Lin-Tsay shell element formulation. Considering the dimensions of the weld and the HAZ softening zone, a mesh size of 4 mm was selected for the specimen. A larger mesh size would fail to capture detailed deformation within the weld zone, while a smaller mesh size would produce elements thinner than the plate thickness, potentially causing simulation errors when using shell elements and greatly increasing computational costs. Contact between the indenter and the specimen was modeled with automatic surface-to-surface contact and a friction coefficient of 0.3. The indenter was defined as a rigid body (Mat. 020-rigid) to prevent deformation during the simulation.

To accurately depict the boundary conditions, the steel frame was modeled using shell elements with an 8 mm element size. The material was assumed to be elastic-perfectly plastic, with a Young's modulus of 210 GPa, a Poisson's ratio of 0.3, and a yield stress of 235 MPa. For simplicity, the bolts attaching the top and bottom frames were not explicitly modeled; instead, multiple point constraints (MPCs) were applied between the frames and the specimen at the bolt hole locations.

To account for the anisotropic properties of the material, the Hill (1948) yield criterion and the associated flow rule were adopted. Under plane stress conditions, the yield function is expressed as:

$$\overline{\sigma}_H^2 = F\sigma_{yy}^2 + G\sigma_{xx}^2 + H\left(\sigma_{xx} - \sigma_{yy}\right)^2 + 2N\sigma_{xy}^2 \tag{1}$$

where F、G、H、N are anisotropic parameters which can be obtained from tensile tests along different directions, and the relationship between parameters and Lankford coefficients is:

$$\begin{aligned} F &= \frac{r_0}{r_{90}(r_0+1)}, \mathrm{G} = \frac{1}{r_0+1} \\ H &= \frac{r_0}{r_0+1}, \mathrm{N} = \frac{(r_0+r_{90})(r_{45}+0.5)}{r_{90}(r_0+1)} \end{aligned} \tag{2}$$

Table 4 shows the anisotropic parameters used in the model. For comparison, the final yield surface is shown in Fig. 18, along with the von Mises yield surface under plane stress conditions. As observed, adding anisotropic parameters causes the yield surface to deviate from the isotropic case.

Additionally, isotropic hardening is assumed for the material, meaning that the strain hardening curves are parallel in different di-

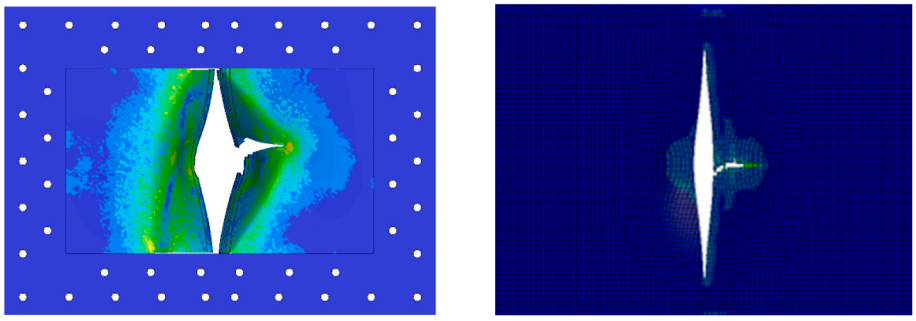

Fig. 29. The comparison of deformation and failure mode results.

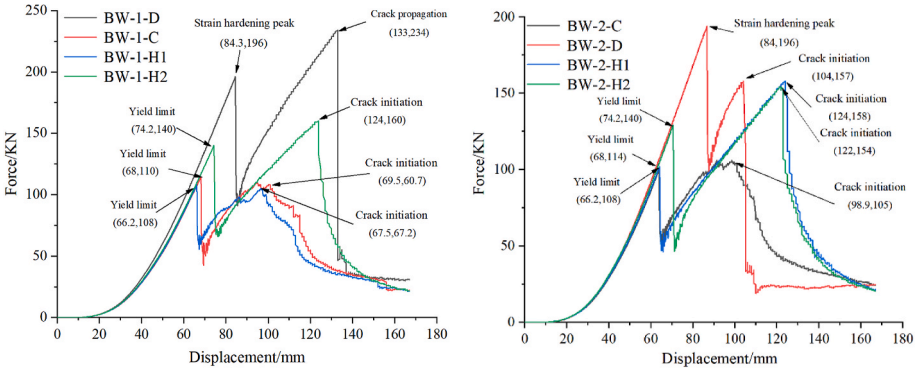

(1) One butt weld plate (2) Two butt weld plates

Fig. 30. Comparison of results at different punching positions.

rections. This assumption is supported by the observation that the stress–strain curves for specimens in various orientations are almost identical. As a result, the hardening behavior is described by a power law relationship.

$$\sigma_t = K\varepsilon_t^n \tag{3}$$

where parameters K and n are determined by the extrapolation of the accurate stress-strain data before necking (Liu et al., 2013).

The softening effect caused by welding is also considered. The areas surrounding the weld are shown in Fig. 19 and are divided into four distinct zones: base metal, HAZ 1, HAZ 2, and the weld zone. Based on hardness measurements and mesh size, the weld zone is assigned a width of 4 mm on each side, while its thickness is determined to be 5.2 mm using the area equivalence method (Liu et al., 2015c). The total width of the HAZ is set at 36 mm according to hardness test results. Due to significant variations in material properties within the HAZ, this region is further divided into two zones—HAZ 1 (20 mm wide) and HAZ 2 (16 mm wide)—based on hardness values.

Based on the correlation between hardness values and material strength, the engineering stress–strain curves for different regions were derived by interpolating tensile test results from both the base material and the small welded specimens (Specimen I). Figs. 20 and 21 show the average hardness values and the corresponding actual stress–strain relationships for the base metal, HAZ, and weld zones.

The material model used is Mat. 041 (user-defined material model), with the true failure strain determined by conducting successive tensile simulations until the numerical results match the corresponding experimental engineering fracture strain. Fig. 22 presents the engineering stress–strain curves for the HAZ 1 material, obtained from both experimental data and numerical simulations. The true failure strain for HAZ 1 is identified as 0.21 when the mesh size is 4 mm. Further details can be found in Lu et al. (2021).

4.2. Comparison results

(1) Comparison of Experimental and Numerical Damage Patterns

The results from both experiments and simulations are shown in Fig. 23. It is clear that the numerical models accurately predict the impact responses. In some cases, the numerically calculated structural stiffness is slightly underestimated, particularly during the initial penetration phase. This discrepancy mainly arises from simplifying the material properties near the weld, since the material curves for different regions are obtained through interpolation rather than direct tensile testing. Nonetheless, the overall trends and peak force values are well captured by the numerical analysis.

Damage patterns under different impact scenarios are shown in Figs. 24–27, where contour plots indicate the distribution of plastic strain. For the BW-1-C case, the fracture begins in the HAZ 1 region, as shown in Fig. 24a. As indentation continues, longer cracks develop in the highly deformed areas compared to the experiment, causing a sharp decrease in resistance force due to the simultaneous removal of multiple elements. Additionally, a crack forms in the orthogonal direction, resulting in a complete loss of load-carrying capacity in the specimen. This behavior is well reproduced by the finite element model, as illustrated in Fig. 24b. In contrast, for the specimen with two butt welds (BW-2-D), where the indenter impacts the weld seam, fracture first occurs in the HAZ at the impact site, and the specimen immediately loses its load-bearing capacity, which aligns with the experimental results.

When the indenter does not impact the weld seam (BW-1-D and BW-2-C), noticeable ductile deformation occurs, creating a necking circle in the simulations. Fracture begins in the HAZ area near the weld, which aligns well with the test results (Figs. 25 and 26).

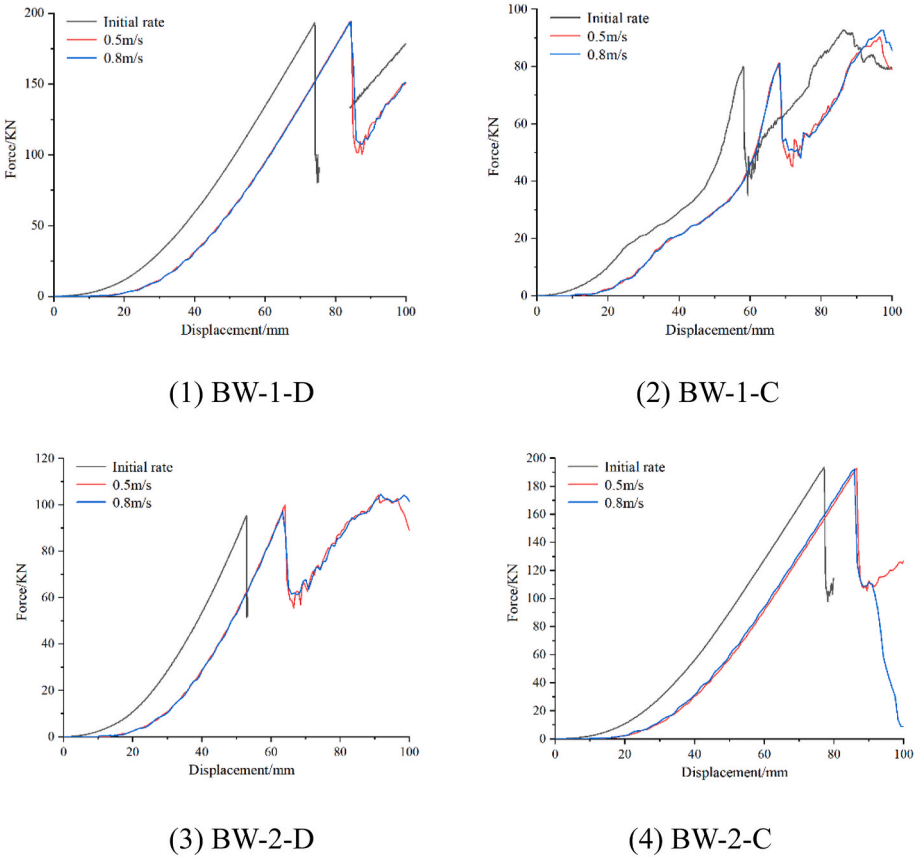

Fig. 31. Comparison of results under different loading rates.

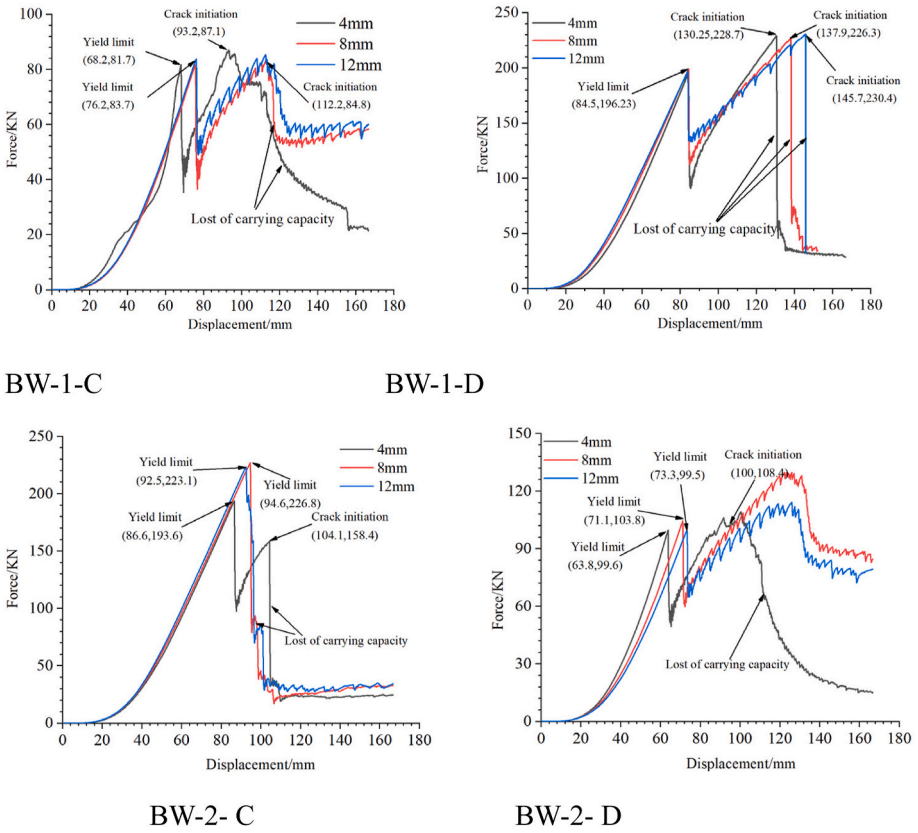

Fig. 32. Mesh sensitivity of force–displacement for four welded-plate cases (4/8/12 mm).

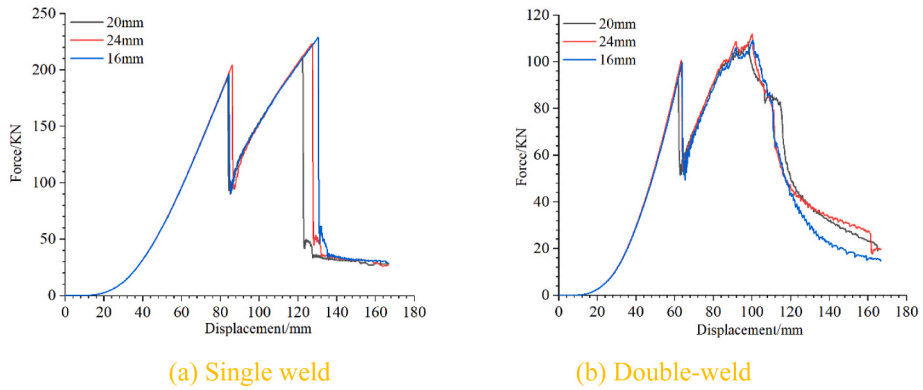

Fig. 33. Comparative analysis of the results of double weld with and without initial deformation/stress.

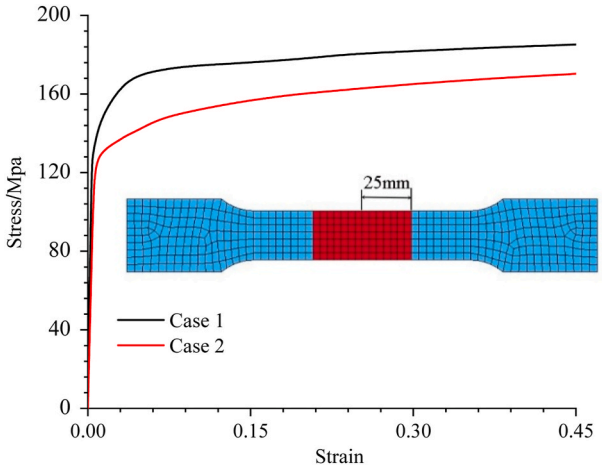

Fig. 34. Numerical modelling of HAZ softening zone and the hardening curves.

(2) Comparison of Dynamic Drop-Weight Impact and Quasi-static Indentation

The comparative analysis of quasi-static and dynamic loading reveals notable differences in material response and failure mechanisms. For example, aluminium alloys are sensitive to strain rate changes, leading to higher strengths and potentially different fracture behavior under dynamic or impact loading. Additionally, welded zones—especially the heat-affected zone (HAZ)—may experience localized brittle fracture at high strain rates. Therefore, this study conducted both quasi-static and drop-weight dynamic simulations on plates with single butt welds, at loading rates of 0.16 m/s and 3 m/s, respectively.

As shown in Fig. 28, the force–displacement curves from dynamic drop-weight impact and quasi-static indentation tests clearly illustrate how strain rate affects the mechanical response of welded aluminum alloys. Under dynamic loading, the peak load of the structure is much higher than under quasi-static conditions, emphasizing the material's sensitivity to strain rate. The dynamic impact curve rises more sharply and shows a quick drop after reaching the peak, indicating a higher likelihood of brittle or localized failure and less plastic deformation. In contrast, the quasi-static curve displays a smoother transition and more noticeable ductile deformation.

Additionally, the area enclosed by the dynamic impact curve is larger, indicating an improved energy absorption capacity at high strain rates. However, in extreme cases, material ductility decreases, and failure occurs more suddenly, with the heat-affected zone (HAZ) of the welded joint being especially vulnerable to brittle fracture.

As shown in Fig. 29, during quasi-static indentation, the structural deformation is more consistent, with fracture mainly driven by ductile stretching and slow crack growth, especially near the heat-affected zone (HAZ). In contrast, under dynamic or impact loading, inertia and thermal effects often cause localized shear bands, adiabatic softening, and even quasi-brittle fracture. The paths of crack initiation and growth may also vary under these conditions.

This study only considers quasi-static loading conditions, which differ to some extent from the dynamic or impact scenarios encountered in actual engineering applications. Under dynamic loading, welded aluminum plates may exhibit different strain rate effects and damage mechanisms. Therefore, the present work provides fundamental data and modeling references for structural response under quasi-static conditions. Future research should include experimental and simulation analyses under high strain rate or impact loading to achieve a more comprehensive assessment of structural safety.

(3) Different indentation positions

To improve the thoroughness of the investigation, we systematically examined the effects of different indentation positions, loading rates, and anisotropy coefficients on the structural response of stiffened plate specimens. Specifically, for indentation position, three distinct scenarios were designed based on the relative location of the indenter: Scenario 1: Quasi-static indentation with the indenter at the geometric center of the plate specimen. Scenario 2: Quasi-static indentation with the indenter offset 125 mm from the plate center (relative to Scenario 1). Scenario 3: Quasi-static indentation with the indenter directly aligned above the weld seam.

As shown in Fig. 30, the results indicate that the base metal region exhibits the highest peak load and the longest displacement path, demonstrating excellent ductility and strength. As the primary load-bearing area of the structure, the base metal significantly surpasses the other zones. In contrast, the weld region shows a notable reduction in resistance due to metallurgical changes and the buildup of potential defects, making it more vulnerable to early plastic instability or brittle fracture. The heat-affected zone (HAZ) acts as a transition area in terms of mechanical properties, marked by both softening effects and increased crack sensitivity. Within the HAZ, HAZ-1 (next to the weld center) shows clear softening and a substantial drop in strength. Conversely, HAZ-2 (further from the weld center) gradually approaches the strength of the base metal, with its mechanical properties progressively improving (see Fig. 31).

(4) Different loading rates

To assess how different loading rates affect test results, indentation experiments were performed at three rates: 0.166 m/s, 0.5 m/s, and 0.8 m/s. In all cases, the peak load of the aluminum plate specimens stayed around 230 kN, with only minor differences. As the loading rate

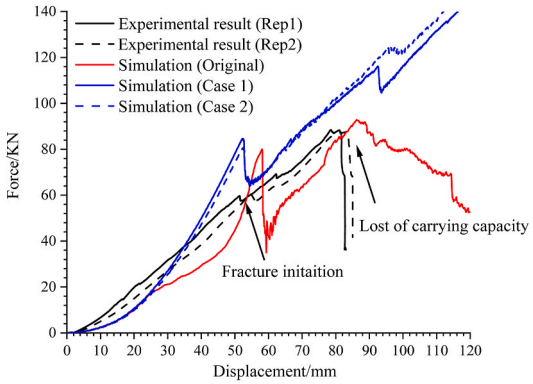

(a) Impact responses

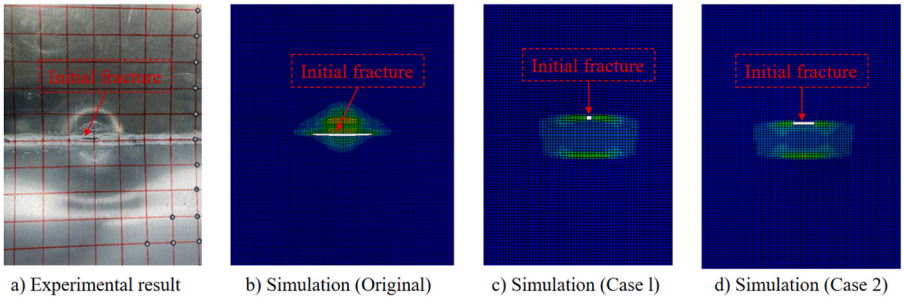

a) Experimental result b) Simulation (Original) c) Simulation (Case l) d) Simulation (Case 2)

(b) Damage shapes when the fracture initiates

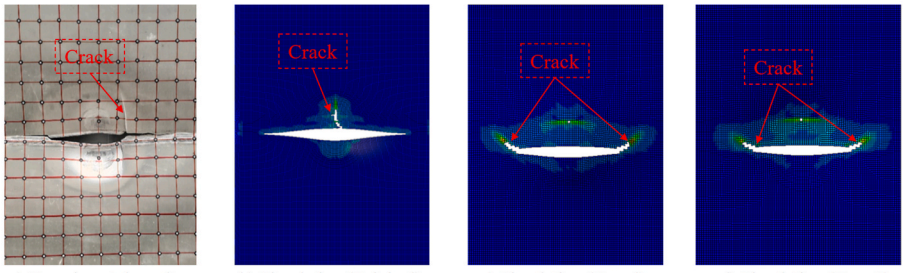

a) Experimental result b) Simulation (Original) c) Simulation (Case l) d) Simulation (Case 2)

(c) Damage shapes when losing carrying capacity

Fig. 35. Comparison results of BW-1-C from different HAZ modelling approaches.

increased, there was a slight rise in peak displacement, indicating a small improvement in the material's deformation capacity at higher strain rates. The energy absorption capacity (shown by the area under the curve) showed limited change across the rates, suggesting that, under these experimental conditions, the strain rate strengthening effect is not significant and the overall resistance to impact remains fairly consistent.

(5) Different mesh size

In order to verify the influence of mesh size on the results, we used three uniform shell element sizes: 12 mm, 8 mm and 4 mm (the same 4-node shell as the main model, with five thickness integration points and the same material, contact and boundary definitions) to perform a special mesh sensitivity analysis on all four welded plate configurations (BW-1-C, BW-1-D, BW-2-C, BW-2-D).

As shown in Fig. 32, across all four welded-plate configurations (BW-1-C, BW-1-D, BW-2-C, BW-2-D), refining the shell mesh from 12 mm to 8 mm and 4 mm results in nearly identical force–displacement curves: the peak force differs by only approximately 3–5 %, crack-initiation/fracture displacement by about 4–6 %, and the yield onset ("knee") is captured within roughly 2–3 %. The equivalent-plastic-strain fields display the same necking circle beneath the indenter, the same first crack site in the HAZ next to the weld, and the same propagation direction across all meshes; the finer mesh simply reduces the size of the localisation band and sharpens the post-peak softening, as expected. Therefore, a 4 mm production mesh is adopted because it captures the weld and HAZ sub-zones (weld approximately 4 mm per side; HAZ-1 approximately 20 mm; HAZ-2 approximately 16 mm) with multiple elements, reproduces peak load and fracture displacement within a few percent of coarser meshes, and offers a good balance between accuracy and computational cost, confirming that the global response and failure mechanisms are insensitive to mesh size.

(6) Different HAZ width

To assess robustness with respect to the extent of the softening zone. We performed a HAZ-width sensitivity analysis for both single-and

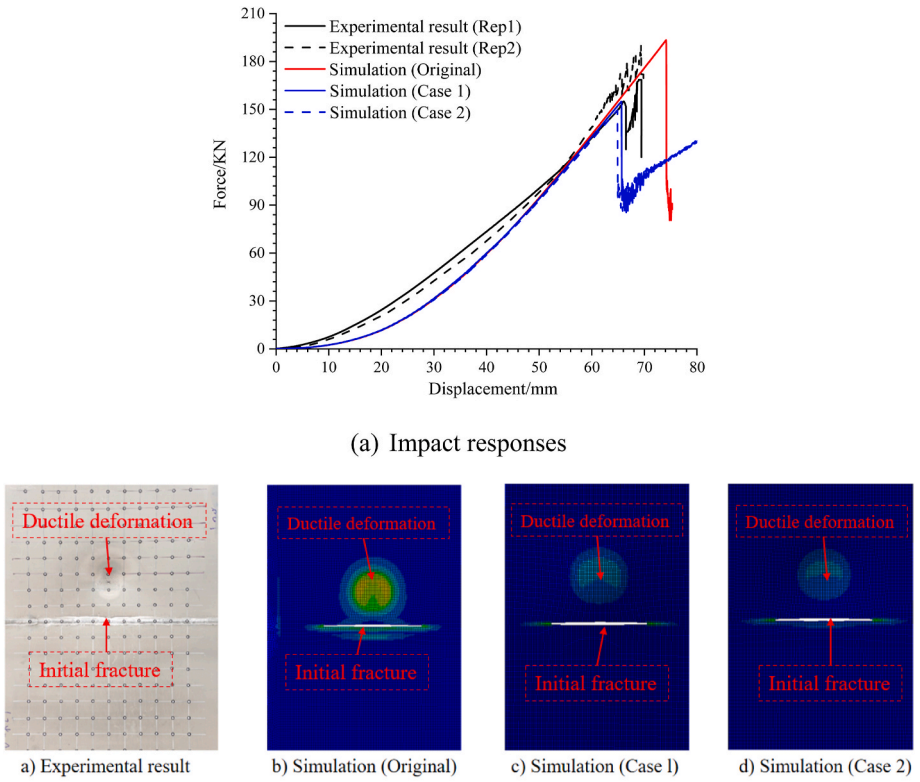

Fig. 36. Comparison results of BW-1-D from different HAZ modelling approaches.

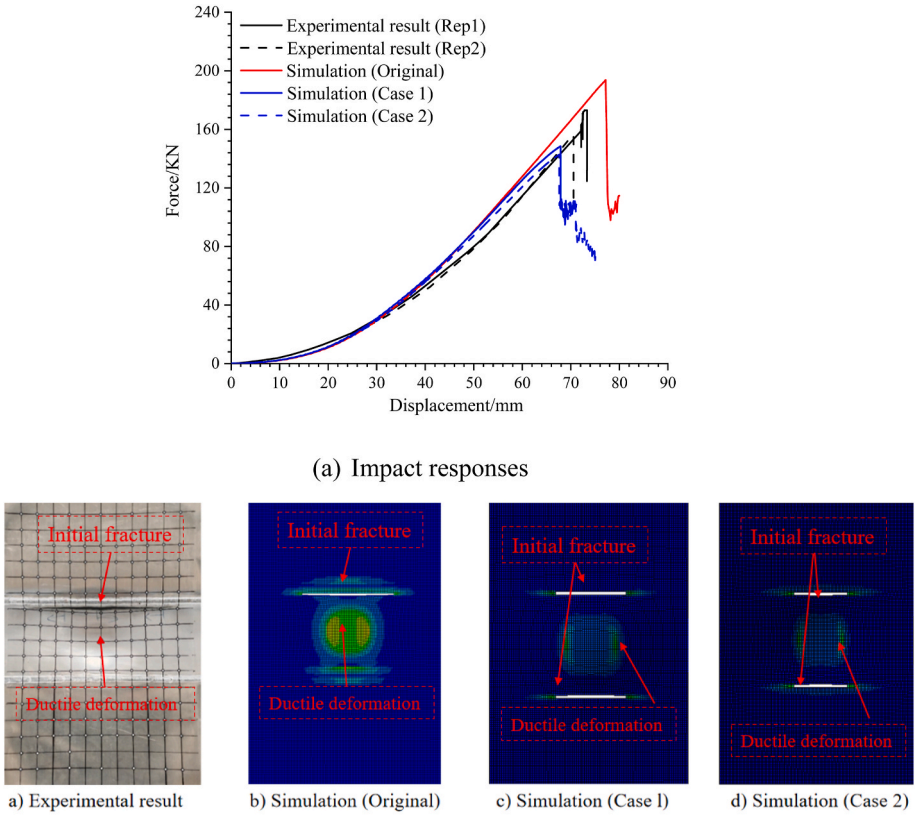

Fig. 37. Comparison results of BW-2-C from different HAZ modelling approaches.

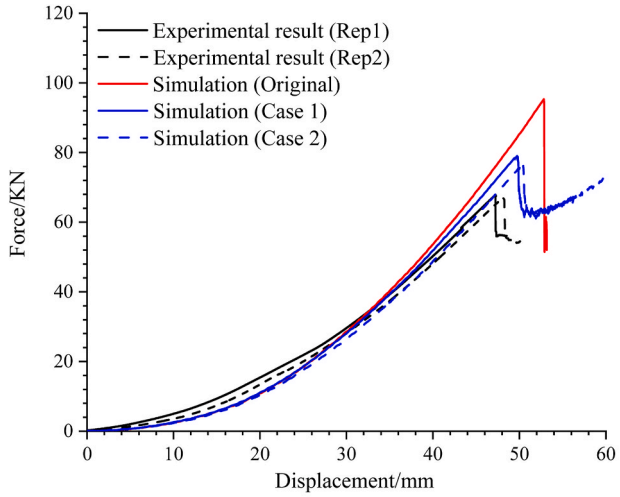

(a) Impact responses

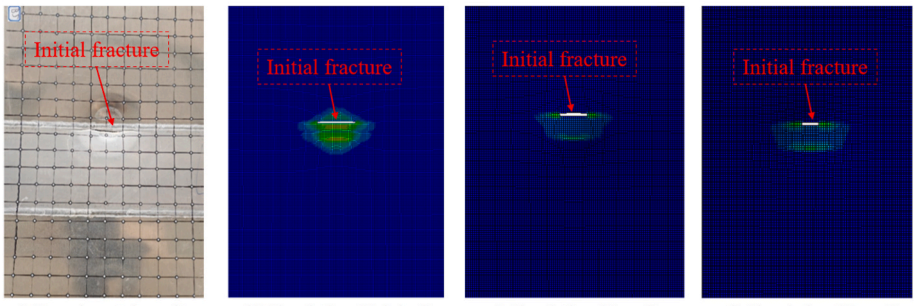

(b) Damage shapes

Fig. 38. Comparison results of BW-2-D from different HAZ modelling approaches.

double-weld plates by comparing 16 mm, 20 mm and 24 mm assumptions. According to the welding hardness distribution diagram in Fig. 3, the hardness of the HAZ of 20 mm and 24 mm was re-determined, and the stress-strain curve of the HAZ region was re-determined. The calculated force-displacement curves of different HAZ widths are shown in Fig. 33.

The results of this parametric study show only minor changes in the predicted peak loads and fracture displacements (differences were within ~5 %). The overall failure modes and damage patterns remained the same for HAZ widths in this range. These findings suggest that our model's predictions are robust against moderate variations in HAZ extent.

4.3. Discussion

As previously mentioned, much of the existing literature and relevant codes provide empirical methods for assessing the extent and severity of HAZ softening. In this study, two commonly used HAZ modeling methods are employed in the numerical simulations to analyze their impact on the predicted response of welded aluminum specimens.

In Case 1, the width of the HAZ is assumed to be 25 mm from the weld reference point. A single set of material parameters is used, and the mechanical properties are determined through a reverse engineering method based on the cross-weld tensile test. Both the hardening and fracture parameters are obtained by iteratively comparing the experimental and numerical results of the tensile test. The anisotropic parameters for this region are set to be the same as those of the base material. The final failure strain is determined to be 0.42, and the corresponding hardening curve is presented in Fig. 34.

In Case 2, the HAZ width is also assumed to be 25 mm. The hardening curve for the HAZ region is determined using a knock-down factor recommended by DNV. According to this recommendation, the reduced proof strength of the HAZ in 6061-T6 aluminum can be taken as 0.48 times the strength of the base material, as shown in Fig. 34. Since no relevant fracture parameter data for the HAZ zone are available in the literature, the fracture parameters are assumed to be the same as those used in Case 1.

The comparison results from different HAZ modeling approaches are shown in Figs. 35–38. As can be seen, the differences in predictive results between case 1 and case 2 are minimal, indicating that the simplified method recommended by DNV can serve as a good alternative to methods based on cross-weld tensile tests. However, the codes do not provide guidance regarding fracture parameters, as they focus on the ultimate strength of welded aluminum. The fracture strain of the softening zone assumed in this study is considered a useful reference for future studies involving accidental analysis.

In the case of BW-1-C, it is clear that the results from cases 1 and 2 cannot accurately assess the impact responses and the damage patterns, especially when the specimen loses its load-bearing capacity. As shown in Fig. 35a, the impact responses from cases 1 and 2 display higher structural stiffness than the actual test. At the onset of fracture, no significant necking circle appears at the impact location in cases 1 and 2, and deformation is focused at the edge of the modeled HAZ zone. Subsequently, a large crack forms in the HAZ region, but an orthotropic

crack does not develop around the necking circle. Instead, the crack propagates within the confined area of the HAZ zones, causing the impact force to continue increasing even after a 90 mm displacement.

In the remaining cases where the tests stop at fracture initiation, impact force responses from cases 1 and 2 generally align with the simulation results from the original methods, except for slight differences in fracture displacement. However, noticeable scatter exists in the damaged shapes when different modeling methods are used. No clear strain concentration occurs in the impact area to form a necking circle in these cases. This is because the material properties of the weld and HAZ zones are assumed to be homogenized, and this simplified modeling approach cannot accurately capture the strain concentration characteristics of welded aluminum structures under impact loads.

In conventional simulation methods, the HAZ is usually simplified as a single region or treated uniformly with empirical formulas. Common examples include the widely used "one-inch rule," the empirical reduction factor method, and assigning a single set of material parameters. However, these methods overlook local variations in material properties within the weld area and its surroundings, making it challenging to accurately capture the actual failure behavior of welded structures under collision loads. In this study, a new, detailed modeling approach for the weld HAZ is proposed, incorporating hardness gradients and localized tensile tests. The hardness test clearly distinguishes the base metal, weld metal, and HAZ. The HAZ is further divided into multiple sub-regions (e.g., HAZ-1, HAZ-2), and miniature tensile tests at various distances from the weld provide the distribution of material properties. An accurate relationship between hardness and strength is established, allowing point-by-point definition of material properties within the HAZ. This detailed method greatly enhances the accuracy of ship collision simulations in predicting structural failure modes and local load-bearing capacities, surpassing the limitations of traditional single-region or empirical modeling techniques.

In this work we did not explicitly model welding-induced residual stresses or initial out-of-plane distortions because specimen-specific fields were unavailable and our primary objective was to isolate and quantify HAZ softening; moreover, under quasi-static indentation the large plastic strains rapidly relax pre-stresses, so their influence on the global response is expected to be limited. Targeted with/without checks using representative residual-stress fields and a saddle-shaped imperfection confirmed that the governing HAZ-controlled localisation and failure path are unchanged; the main effect is a slightly earlier local yielding with a narrower localisation band, while peak load and fracture displacement vary only marginally (order of a few percent). We therefore consider the omission acceptable for the present scope, with negligible impact on the conclusions. Nevertheless, for weldments with unusually high heat input, for stability-dominated problems, or under high-rate loading, residual stresses and distortions may play a larger role; future work will incorporate specimen-specific fields obtained from measurement or dedicated welding simulations.

5. Conclusions

This paper presents both experimental and numerical investigations on welded AA6061-T6 aluminum plates subjected to impact loading. The study thoroughly examines the effect of welding-induced softening on the structural response. The main conclusions from this research are as follows:

1. The presence of weld seams in aluminum structures significantly affects their impact responses. When the indenter strikes the weld, the specimen typically shows reduced fracture displacement and lower structural resistance. Additionally, noticeable ductile deformation occurs beneath the indenter, with fracture consistently starting in the HAZ region next to the weld.
2. The results show that numerical models with a detailed representation of the softening zone in welded aluminum structures can accurately predict both the indentation force responses and the resulting damage patterns.
3. For aluminum structures experiencing complex deformation processes, like crack propagation, empirical methods—such as the one-inch rule—fail to accurately capture damage characteristics, mainly because of the homogenization of material properties within the softening zone.
4. In cases where detailed material properties of welded aluminum alloys are not available, the knock-down factor method recommended by DNV is a practical alternative to approaches based on cross-weld tensile tests. However, more research on fracture parameters is needed to enhance guidance for the accidental analysis of aluminum structures.

CRediT authorship contribution statement

Shuai Zong: Writing – original draft. **Yue Lu:** Methodology. **Kun Liu:** Funding acquisition. **Zili Wang:** Formal analysis. **Bai-Qiao Chen:** Writing – review & editing. **C. Guedes Soares:** Writing – review & editing.

Declaration of competing interest

We would like to submit the enclosed manuscript entitled “Experimental and numerical study on welded aluminum plates under quasi-static impact loads”. I would like to declare on behalf of my co-authors that there are no known conflicts of interest associated with this publication. All the authors listed have approved the manuscript is enclosed.

Acknowledgements

We gratefully acknowledge the financial support of the National Natural Science Foundation of China (Grant No. 52271279; 52171311). This work contributes to the Strategic Research Plan of the Centre for Marine Technology and Ocean Engineering (CENTEC), which is financed by the Portuguese Foundation for Science and Technology (Fundação para a Ciência e Tecnologia - FCT) under contract UIDB/UIDP/00134/2020. This paper was funded by the Jiangsu Government Study Abroad Scholarship.

References

ABS, 2012. Guide for building and classing high-speed craft. Am. Bureau Ship. Houston.
British Standard, 1991. BS8118 - the Structural Use of Aluminium. British Standards Institution.
British Standard, 2007. Eurocode 9—Design of Aluminium Structures. British Standards Institution.
CEN/TC 250, 2023. EN 1999 Eurocode 9: Design of Aluminium Structures (Second Generation). European Committee for Standardization.
Cerik, B.C., 2017. Damage assessment of marine grade aluminium alloy-plated structures due to air blast and explosive loads. Thin-Walled Struct. 110, 123–132.
Chen, B.Q., Guedes Soares, C., 2019. Numerical investigation on weld-induced imperfections in aluminum ship plates. J. Offshore Mech. Arctic Eng. 141 (6), 061605.
Chen, B.Q., Liu, K., Xu, S., 2024. Recent advances in aluminum welding for marine structures. J. Mar. Sci. Eng. 12 (9), 1539.
Collette, M., 2005. The Strength and Reliability of Aluminium Stiffened Panels. Newcastle University. Ph.D. thesis.
Dunand, M., Maertens, A.P., Luo, M., Mohr, D., 2012. Experiments and modeling of anisotropic aluminum extrusions under multi-axial loading – part I: plasticity. Int. J. Plast. 36, 34–49.
Gupta, S., Singh, D., Yadav, A., Jain, S., Pratap, B., 2020. A comparative study of 5083 aluminium alloy and 316L stainless steel for shipbuilding material. Mater. Today Proc. 28, 2358–2363.
Hosseinabadi, O.F., Khedmati, M.R., 2021. A review on ultimate strength of aluminium structural elements and systems for marine applications. Ocean Eng. 232, 109153.
Kaufman, J.G., 2000. Introduction to Aluminum Alloys and Tempers. ASM International.
Khedmati, M.R., Pedram, M., Rigo, P., 2014. The effects of geometrical imperfections on the ultimate strength of aluminium stiffened plates subject to combined uniaxial compression and lateral pressure. Ships Offshore Struct. 9, 88–109.

Koubaa, S., Mars, J., Wali, M., Dammak, F., 2016. Numerical study of anisotropic behavior of aluminum alloy subjected to dynamic perforation. Int. J. Impact Eng. 101, 105–114.
Lai, Y.F.W., 1989. Buckling Strength of Welded and Non-welded Aluminium Members. University of Sheffield. Ph.D. thesis.
Li, C.F., Ren, H.L., Zhu, Z.Y., Feng, G.Q., Fu, P., Guedes Soares, C., 2020. Influence of model extension and boundary conditions on the buckling behaviour of aluminium integrally stiffened panels under uniaxial compressive loading. Ocean Eng. 216, 108066.
Li, B., He, P., Wang, J., Pan, X., Wang, Y., Wang, Z., Baniotopoulos, C.C., 2024a. Mechanical characteristic and stress-strain modelling of friction stir welded 6061-T6 aluminium alloy butt joints. Thin-Walled Struct. 198, 111645.
Li, B., Li, G., Wang, J., Chen, B., Wang, Y., Dai, Y., Dong, G., 2024b. Residual stress tests and predictive model of friction stir welded normal-strength aluminium alloy H-shaped sections. Eng. Struct. 319, 118789.
Li, B., Shen, F., Wang, J., Zhi, X., Wang, Y., Lin, S., Ouyang, Y., 2024c. Experimental study on mechanical behaviour of friction stir welded aluminium alloy butt joints. In: Structures, 63. Elsevier, 106407.
Liu, B., Guedes Soares, C., 2015. Plastic response and failure of rectangular cross-section tubes subjected to transverse quasi-static and low-velocity impact loads. Int. J. Mech. Sci. 90, 213–227.
Liu, B., Villavicencio, R., Guedes Soares, C., 2013. Experimental and numerical plastic response and failure of pre-notched transversely impacted beams. Int. J. Mech. Sci. 77, 314–332.
Liu, B., Villavicencio, R., Guedes Soares, C., 2014. On the failure criterion of aluminum and steel plates subjected to low-velocity impact by a spherical indenter. Int. J. Mech. Sci. 80, 1–15.
Liu, B., Villavicencio, R., Guedes Soares, C., 2015a. Influence of striker shape on the crack initiation and propagation on laterally impacted thin aluminium plates. J. Offshore Mech. Arctic Eng. 137 (5), 051402.
Liu, B., Villavicencio, R., Guedes Soares, C., 2015b. Shear and tensile failure of thin aluminium plates struck by cylindrical and spherical indenters. Ships Offshore Struct. 10 (1), 45–58.
Liu, B., Dong, A., Villavicencio, R., Liu, K., Guedes Soares, C., 2020a. Experimental and numerical study on the penetration of stiffened aluminium alloy plates punched by a hemi-cylindrical indenter. Ships Offshore Struct. 15, 1–14.
Liu, B., Liu, K., Villavicencio, R., Dong, A., Guedes Soares, C., 2020b. Experimental and numerical analysis of the penetration of welded aluminium alloy panels. Ships Offshore Struct. 15, 1–13.
Liu, B., Chen, C., Garbatov, Y., 2022. Material failure criterion in the finite element analysis of aluminium alloy plates under low-velocity impact. Ocean Eng. 266, 113260.
Lu, Y., Liu, K., Wang, Z., Tang, W., 2021. Modelling of ductile fracture in ship structures subjected to quasi-static impact loads. Int. J. Impact Eng. 156, 103941.
Magoga, T., Flockhart, C., 2014. Effect of weld-induced imperfections on the ultimate strength of an aluminium patrol boat determined by the ISFEM rapid assessment method. Ships Offshore Struct. 9, 218–235.
Mazzolani, F.M., 2014. Aluminium Structural Design. Springer, London.
Morin, D., Kaarstad, B.L., Skajaa, B., Hopperstad, O.S., Langseth, M., 2017. Testing and modelling of stiffened aluminium panels subjected to quasi-static and low-velocity impact loading. Int. J. Impact Eng. 110, 97–111.
Paik, J.K., Duran, A., 2004. Ultimate strength of aluminum plates and stiffened panels for marine applications. Mar. Technol. 41, 108–121.
Paik, J.K., Hughes, O.F., Hess, P.E., et al., 2005. Ultimate limit state design technology for aluminum multi-hull ship structures. In: SNAME Maritime Convention. SNAME. D021S003R002.
Quach, H., Kim, Y.-S., 2021. Effect of non-associated flow rule on fracture prediction of metal sheets using a novel anisotropic ductile fracture criterion. Int. J. Mech. Sci. 195, 106224.
Rahmaan, T., Noder, J., Abedini, A., Zhou, P., Butcher, C., Worswick, M.J., 2020. Anisotropic plasticity characterization of 6000- and 7000-series aluminum sheet alloys at various strain rates. Int. J. Impact Eng. 135, 103390.
Rønning, L., Aalberg, A., Larsen, P.K., 2010. An experimental study of ultimate compressive strength of transversely stiffened aluminium panels. Thin-Walled Struct. 48, 357–372.
Veritas, D.N., 2001. Rules for Ships: High Speed, Light Craft and Naval Surface Craft. Det Norske Veritas.
Villavicencio, R., Sutherland, L.S., Guedes Soares, C., 2012. Numerical simulation of transversely impacted, clamped circular aluminium plates. Ships Offshore Struct. 7 (1), 31–45.
Zha, Y., Moan, T., 2001. Ultimate strength of stiffened aluminium panels with predominantly torsional failure modes. Thin-Walled Struct. 39, 631–648.